JOURNAL OF PROPULSION AND POWER
Vol. 22, No. 5, September–October 2006

Experimental and Computational Investigation of Light-Gas Injectors in Mach 4.0 Crossflow

Luca Maddalena,* Theresa L. Campioli,* and Joseph A. Schetz†
Virginia Polytechnic Institute and State University, Blacksburg, Virginia 24060

An experimental and computational study of an aerodynamic ramp (aeroramp) injector was conducted at Virginia Polytechnic Institute and State University. The aeroramp consisted of an array of two rows with two columns of flush-wall holes that induce vorticity and enhance mixing. The holes were spaced four diameters apart in the streamwise direction with two diameters transverse spacing between them. For comparison, a single-hole circular injector with the same area angled downstream at 30 deg was also examined. Test conditions involved sonic injection of helium heated to 313 K to safely simulate hydrogen into a Mach 4 air cross stream with average Reynolds number 5.77 e + 7 per meter at a jet to freestream momentum flux ratio of 2.1. Sampling probe measurements were utilized to determine the local helium concentration. Pitot and cone-static-pressure probes and a diffuser thermocouple probe were employed to document the flow. This allowed total pressure losses to be determined. The numerical flow solver used was GASP v. 4.2. The inviscid fluxes were computed in three dimensions using third-order AUSM+ with modified essentially nonoscillatory limiting. The AUSM+ algorithm was chosen because of its good resolution of shock discontinuities and its efficiency. The Wilcox k-ω (1998) turbulence model was used. The main results of this work can be summarized as follows: 1) the mixing efficiency value of this aeroramp design, which was optimized at Mach 2.4 for hydrocarbon fuel, was only slightly higher than that of the single-hole injector at these flow conditions; 2) the mass-averaged total pressure loss parameter showed that the aeroramp and single-hole injectors had the same overall losses; 3) the computational fluid dynamics (CFD) was unable to accurately predict the quantitative mixing data produced by the experiment, however, the qualitative comparisons of the injectors using the CFD predictions agreed with the experiment.

Nomenclature

A_j = injector area
C_d = discharge coefficient
d_{eff} = effective diameter
d_{eq} = equivalent diameter
d_j = jet diameter
f = stoichiometric hydrogen-air ratio
M = Mach number
p = (static) pressure
p_c = cone-static pressure
p_t = total pressure
$p_{\text{t,pitot}}$ = pitot pressure
$\bar{q}$ = jet-to-freestream momentum flux ratio
R = resistance
T = temperature
u = flow velocity
V = voltage
x = axial distance downstream of injector center
y = lateral distance from the injector centerline
$y^{\pm}$ = plume width
z = vertical distance from the wall
α = mass fraction
γ = ratio of specific heats
η_m = mixing efficiency
ρ = density

Subscripts

j = jet-exit property
s = system
t = total condition
w = hot film
∞ = freestream property

I. Introduction

BECAUSE of the short fuel residence time inside a scramjet, which is on the order of a millisecond, achieving efficient supersonic combustion forms a challenging problem. Enhanced mixing and rapid combustion imply an increase in combustion efficiency and a reduction of the combustor length, thus reducing the skin-friction drag and increasing the net thrust. For cycle efficiency purposes, the process must also induce low total pressure losses. Mixing enhancement in high-speed flows also has application in a number of other fields such as thermal protection systems and vehicle control by jet thrusters.

A multitude of experiments has been performed in the field of injection in supersonic flow using numerous techniques, such as swept ramps,[1,2] slots,[3,4] transverse injection,[5–10] and jet swirl.[11–16] An extensive review of injector mixing characteristic is given in Schetz et al.[17] The general effects generated by multihole transverse injector arrays have been studied in the design of the aeroramp injector by Cox et al.,[18] Cox and Gruber,[19] R. Fuller et al.,[20] Schetz et al.,[21] and Jacobsen et al.[22,23] The aeroramp was designed to enhance mixing and penetration by inducing a counter-rotating pair of vortices; it showed promising characteristics similar to a physical ramp injector, but with lower pressure losses.

The purpose of the present research is to determine the effectiveness of the specific aeroramp injector design, initially proposed by Jacobsen et al.[23] for ethylene injection into a $M = 2.4$ flow, now for hydrogen injection into a Mach 4 flow. The aeroramp was tested and compared to a single-hole, low-angled, circular injector at the same nominal Mach 4 cross-stream conditions. The Mach 4 airflow simulates typical conditions to those a scramjet combustor would encounter in Mach 10–12 flight. Heated helium was used to simulate hydrogen fuel.

Presented as Paper 2005-3235 at the AIAA/CIRA 13th International Space Planes and Hypersonics Systems and Technologies Conference, Capua, Italy, 16–20 May 2005; received 26 July 2005; revision received 19 December 2005; accepted for publication 23 December 2005.

*Graduate Research Assistant, Department of Aerospace and Ocean Engineering, 215 Randolph Hall. Member AIAA.

†Fred D. Durham Chair, Department of Aerospace and Ocean Engineering, 215 Randolph Hall. Fellow AIAA.

II. Experimental Setup

A. Test Facilities

Experiments were conducted in the Virginia Polytechnic Institute and State University unheated, blowdown supersonic wind tunnel with test section measuring 23 cm wide by 23 cm high and 30 cm long. A schematic of the wind-tunnel nozzle and test section is shown in Fig. 1. The tunnel was configured with a convergent-divergent nozzle resulting in a nominal freestream Mach number of 4. The wind-tunnel calibration shows a fully developed two-dimensional turbulent boundary layer. Data were acquired on a PC with a 16-channel, 16-bit A/D converter, and a 64-channel multiplexer with a built-in cold-junction compensator for temperature measurements. The tunnel digital feedback control ensured the nominal total pressure was maintained constant at $p_t = 1034$ kPa, with an accuracy of ±1%.

B. Aerodynamic Ramp Injector Model

Figure 2 shows the two injector model inserts used in the present investigation. The top surfaces of the inserts are flush with the tunnel wall. The aeroramp injector had four holes, each one with a diameter d_j of 1.61 mm and a corresponding equivalent jet diameter $d_{\text{eq}} = (4A_j/\pi)^{0.5}$ of 3.23 mm. The geometry consisted of two rows of two round holes, spaced four equivalent diameters, in the streamwise direction and two equivalent diameters laterally between the holes. The first and second pair of injector holes had transverse-injection and toe-in angles of 20 and 40 deg and 15 and 30 deg, respectively. The single-hole, circular injector used as a comparator had the same equivalent diameter and was transversely angled 30 deg relative to the downstream direction.

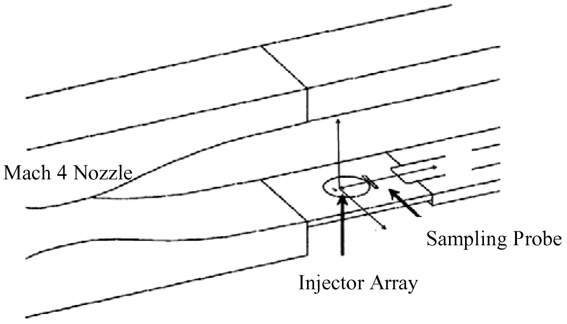

Fig. 1 Virginia Tech test-section setup.

III. Experimental Methods

A. Test Matrix

All wind-tunnel tests were performed at a nominal freestream Mach number of 4.0. Freestream conditions were fixed at a total pressure of 1034 kPa with an ambient mean total temperature of approximately 295 K, producing a freestream Reynolds number of 5.77e + 7 per meter. These conditions resulted in a turbulent boundary layer with a thickness of approximately 20 mm at the point of injection. Heated helium (in order to achieve temperature profiles analogous to the concentration) was used as the injectant to simulate hydrogen fuel. The injectant was heated to an average total temperature of 313 K, and the average injection Mach number was sonic. The jet-to-freestream momentum flux ratio $\bar{q}$ was set to 2.1. Recall that $\bar{q}$ is defined by

$$\bar{q} = \frac{(\rho u^2)_j}{(\rho u^2)_\infty} = \frac{(p\gamma M^2)_j}{(p\gamma M^2)_\infty} \tag{1}$$

A Cartesian coordinate system was chosen with the origin on the wall surface along the test-section centerline, as shown in Fig. 1. The origin of the coordinate system is located on the wall in the middle of the injector array or single injector. The positive x axis is in the freestream direction, the positive z axis is in the vertical direction perpendicular to the wall, and the y axis spans the test section. All lengths are normalized by the effective diameter d_{eff}, defined as

$$d_{\text{eff}} = C_d^{\frac{1}{2}} d_{\text{eq}} \tag{2}$$

where C_d is the injector discharge coefficient. The measured injector discharge coefficients were 0.83 for the aeroramp and 0.88 for the single-hole injector. For the present aeroramp configuration, operating at $\bar{q} = 2.1$, the corresponding helium flow rate was 3.4 g/s. For better comparison, experiments were performed by maintaining the same injectant flow rate.

B. Aerothermodynamic Probing

Aerothermodynamic probing was accomplished by means of pitot, cone-static, and total temperature probes. The pitot probe had an outer diameter of 1.59 mm and an inner diameter of 1.04 mm, which gave a capture area of 0.85 mm^2. The cone-static probe consisted of a cone with a 10-deg half-angle and an outer diameter of 1.59 mm. There were four small ports arranged around the cone to reduce misalignment effects of the probe with respect to the flow. The uncertainty on pressure measurement was evaluated to be ±0.06 atm.

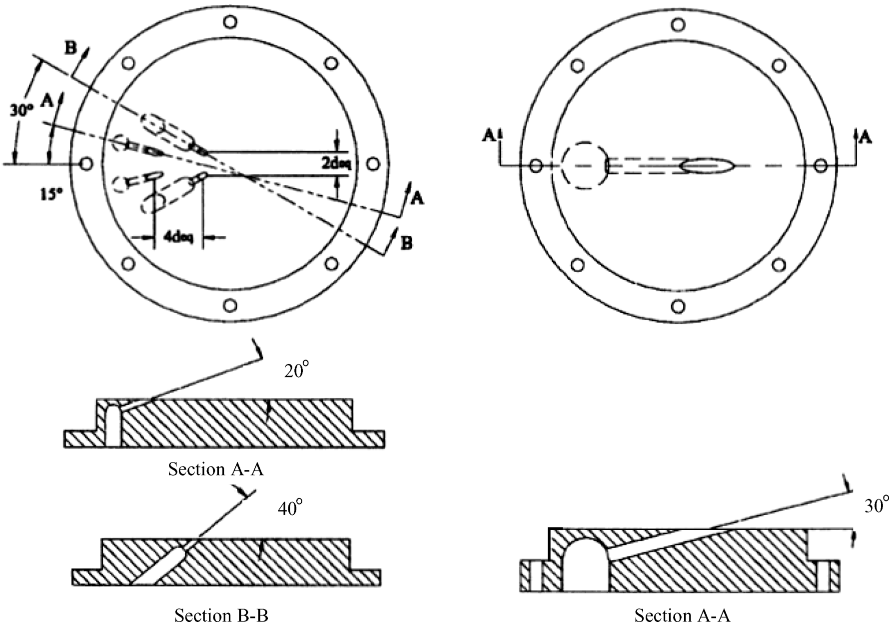

Fig. 2 Injector model inserts. Left is the aeroramp and right is the single-hole injector.

Total temperature was measured with a rake consisting of three tubes of 1.59 mm outer diameter spaced 6.4 mm apart. Each tube had an inner diameter of 1.04 mm giving a capture area of 0.85 mm^2. The total temperature probes also had four small ports to improve the recovery factor. The ratio of capture to recovery area was 5 to 1 resulting in a recovery factor 0.97. Exposed junction type-E thermocouples with 0.25-mm-diam bead were placed inside the three total temperature probes. The uncertainty on temperature measurement was evaluated to be ±2 K.

C. Species Compositions Measurements

Mean species concentration measurements were obtained using an integrated sampling probe and gas analyzer designed specifically for use in supersonic flow. The fundamental concepts and design of this probe were developed at Virginia Polytechnic Institute and State University by W. Ng and his students.[24] The concentration probe is an aspirating type attached to a vacuum pump. The unit consists of a constant temperature hot-film sensor operating in a channel with a choked exit. The hot film has a diameter of 50.8 μm and an active sensor length of 1.02 mm. The probe is designed with a diverging channel between the tip and the sensor plane. The inlet hole at the tip of the probe has the same diameter as the choked orifice, $d = 0.63$ mm. These diameters are chosen so as to preclude the occurrence of a standoff shock at the probe tip. Flow visualization from spark schlieren verified this design intention. The internal probe diameter diverged from 0.63 mm at the inlet to 3.8 mm at the sensor plane, causing a normal shock to occur inside the probe in the diverging channel. In this fashion, a stream tube equal in area to the probe capture area can enter the probe undisturbed. The concentration probe was calibrated to measure the helium molar fraction uniquely related to a given pressure, temperature, and rate of heat transfer sensed at the hot-film operating plane. The absolute measurement uncertainty in helium mass fraction was estimated to be approximately ±7%.

D. Probe Traverse System

For the present investigation, the probes were inserted through the tunnel floor and mounted onto a vertical traversing system. The system traversed a distance of 60 mm in 32 steps, at a speed of 900 steps per second. At each step, the position was maintained for approximately 300 ms. The data for each steps resulted from the average of the last 25 samples of the given step. The vertical traverse velocity was approximately 4.4 mm/s. This setup allowed for the acquisition of a vertical profile with each test run. Between each run, the probe spanwise location was adjusted manually. The uncertainty in probe position was ±0.3 and ±0.2 mm in the cross-stream and vertical positions, respectively.

IV. Data Reduction

A. Concentration Probe

The concentration probe hot-film voltage is related to the Reynolds number by

$$V^2 = [(R_s - R_w)^2/R_w]\pi l\kappa(aRe^b)(T_w - T_t) \tag{3}$$

where R_s, R_w, and l are known, κ is a function of the gas composition, and T_t was measured with an internal thermocouple located at the sensor location. Constants a and b were determined from the concentration probe calibration curves. For each vertical traverse location, a file was generated containing the probe location, sensor voltage, probe total pressure, and probe total temperature. At each point, a computer routine used Eq. (3) with p_t and T_t to calculate the upper and lower voltage bounds, at any given calibration level. The program then would start with the calibration curve of the lowest helium concentration and sequentially search for the two curves that bounded the voltage at the appropriate pressure. The experimental helium concentration was found from interpolation from the bounding curves. Once all of the lateral stations per axial location were reduced, they were put together, and contour plots were generated.

B. Mean Flow Data Reduction

A second code matched the previously calculated helium concentration data to the cone-static pressure, pitot pressure, and total temperature data points in order to calculate profiles for Mach number, density, velocity, mass flux, as well as the flowfield static quantities. Because the ratio of specific heats γ is needed to calculate most of the quantities, it is considered first, and values of $\gamma(y, z)$ and $R(y, z)$ were computed based on the local helium concentration. Next, the remaining flow quantities, M, p and p_t, can be calculated.

The Rayleigh–pitot tube formula relates $p/p_{\mathrm{t,pitot}}$ to M and γ.

$$p/p_{\mathrm{t,pitot}} = f(M, \gamma) \tag{4}$$

This formula assumes a normal shock in front of the pitot probe tip. Using the Taylor–Maccoll equation (solved numerically), it is possible to evaluate the quantity:

$$p_c/p = f(M, \gamma) \tag{5}$$

Taking the ratio of Eqs. (5) and (4), one obtains

$$p_c/p_{\mathrm{t,pitot}} = f(M, \gamma) \tag{6}$$

The left-hand side of Eq. (6) is known because p_c, $p_{\mathrm{t,pitot}}$ were experimentally measured. For each value of γ, a table with the pressure ratio $p_c/p_{\mathrm{t,pitot}}$ and the corresponding Mach number was numerically created using Eq. (6). By comparison with the experimental pressure ratio, the local Mach number was determined. The local speed of sound, velocity, and density were then calculated by use of their respective perfect-gas relations. All calculations assumed a calorically perfect gas with constant specific heats.

V. Experimental Results

All plots presented are from measurements taken at a station 16.4 d_{eff} downstream of the injector. The plots extend $5/d_{\mathrm{eff}}$ on either side of the injector centerline, and data were acquired to an elevation of 18 d_{eff} above the wall. A height of 7 d_{eff} was found to adequately capture the flow characteristics for total temperature, mass fraction, and Mach number, so that data are only presented in this region.

A. Total Temperature Contours

Total temperature profiles for the aeroramp and single-hole injectors are presented in Fig. 3. The local total temperature profiles are normalized by the freestream total temperature, and both profiles are set to the same nondimensional scale for ease of comparison. These isothermal contours illustrate the total temperature field produced by the injection process near the plume of the injector and allow for a qualitative and quantitative assessment of the penetration and mixing produced by the injectors.

An interesting feature of the single-hole injector temperature profile is the horseshoe-shaped structure. This shape is often associated with a vortex structure generated by the interaction of a jet in a crossflow and is the main mechanism for mixing enhancement for this type of injectors. The aeroramp also generates vorticity from the interference effects of the multiple jet interactions and the toe-in angles of the individual jets.

At this point, one might be tempted to estimate mixing performance assuming an analogy between the temperature and the concentration fields. The temperatures in the plume from the aeroramp are lower than those in the circular injector plume, indicating more rapid mixing of the heated helium injectant. One source of error in such an analysis is the total heat loss from the fuel injected from the aeroramp with respect to that injected from the single-hole injector. In the case of the aeroramp, there are four copper feed tubes, each supplying one specific orifice, compared to the single-hole injector, with a single large supply tube. This implies an increase in heat transfer and reduction in injectant temperature caused by the increase of the thermal exchange surface.

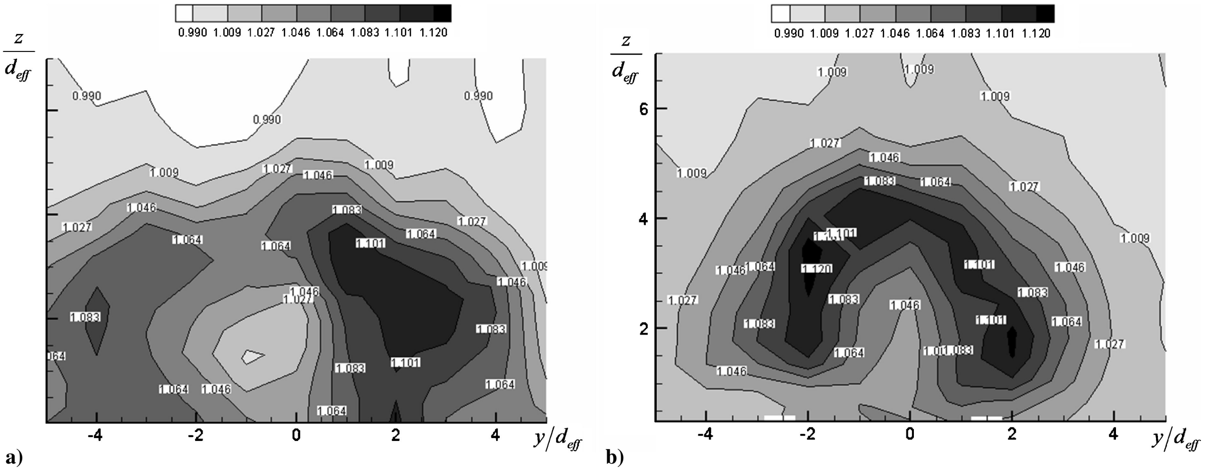

Fig. 3 Normalized total temperature contours $T_t/T_{t,\infty}$ for the a) aeroramp and b) single-hole injectors.

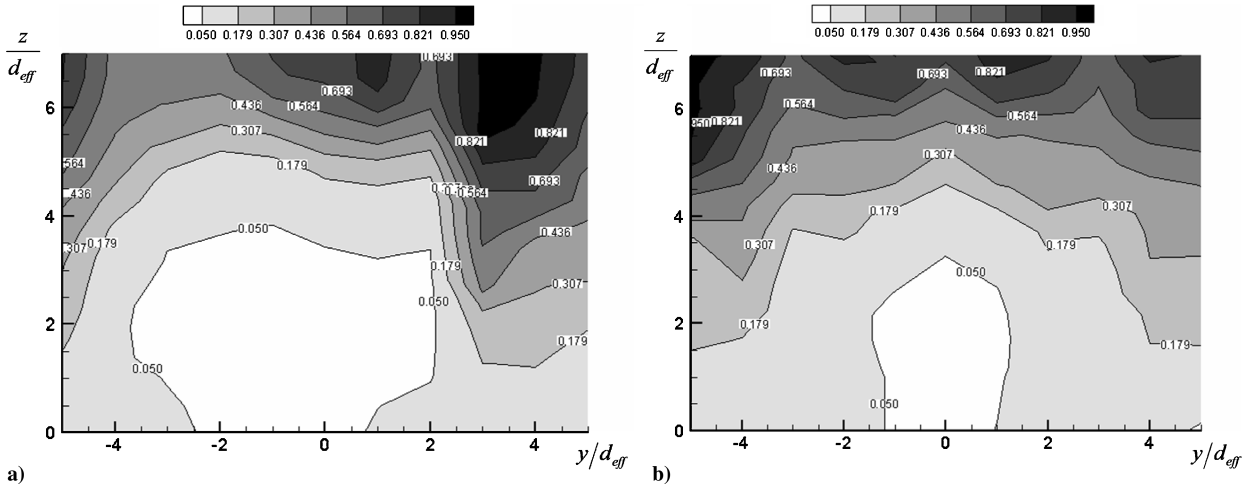

Fig. 4 Normalized total pressure contours $P_t/P_{t,\infty}$ for the a) aeroramp and b) single-hole injectors.

B. Total Pressure Contours and Total Pressure Loss Parameter

Total pressure profiles of the aerodynamic-ramp and single-hole injectors are shown in Fig. 4. These plots show the results from the aerothermodynamic measurement experiments. The local total pressure profiles are normalized by the freestream total pressure (1034 kPa), and both sets of profiles are set to the same nondimensional scale for ease of comparison. These isobar contours illustrate the total pressure field produced by the injection process and allow for a qualitative and quantitative assessment of the losses incurred by the injectors. It can be seen that the aeroramp produced higher local pressure losses in a larger area compared to the single-hole injector. However, the shock from the aeroramp is weaker than that of the single-hole injector. This can be seen in the Mach-number profiles below. The overall total pressure losses are quantified using the overall total pressure loss parameter, which involved numerical integration of the mass-weighted total pressure field over the sampled area. The overall total pressure recovery $P_{\mathrm{t,rec}}$ is defined as[20]

$$P_{\mathrm{t,rec}} = \frac{\int \rho u P \mathrm{d}A}{\int \rho_\infty u_\infty P_{t,\infty}\,\mathrm{d}A + \rho_j u_j P_{t,j} A_j} \tag{7}$$

Then, the total pressure loss parameter is defined as follows; $\Pi = 1 - P_{\mathrm{t,rec}}$. A parameter value of $\Pi = 0$ indicates no total pressure loss, and $\Pi = 1$ indicates complete total pressure loss. Therefore, lower values of Π are better. Table 1 presents the results for the total pressure loss parameter. These results show the aeroramp injector to have only very slightly higher overall losses compared to the single hole. At first glance, this appears in contradiction with the total pressure profiles in Fig. 4 and the preceding comments. However, because the overall total pressure loss parameter is a mass-flow-averaged quantity, the parameter is not assessed on local total pressure alone, but on local density and velocity as well. It turns out that the plume of the aeroramp injector has a higher velocity field in the jet plume. This high velocity field significantly offsets the lower local total pressure.

Table 1 Injectors plume parameters

Parameter	Aeroramp	Single hole
A/A_u	26.4	25.2
z^+	1.75	2
η_m	0.22	0.20
Π	0.389	0.378
$y^\pm$	7.9	6.9

C. Mass Fraction Contours

Helium concentration data are presented in the form of the mass fraction contour plots in Fig. 5. Also indicated are the numerical magnitude of the maximum mass fraction $\alpha_{\max}$ and the location of this local maximum with an × on the contours plots. The minimum contour line ($\alpha = 0.02$) represents the minimum value of concentration measurable in the experiment. The centroid of the lean limit mass fraction for homogeneous H_2-air deflagration at ambient conditions ($\alpha = 0.003$) corresponds to the plume center of mass, and the symbol● marks this position. The contour plots for the aeroramp injector can be seen in Fig. 5a. The core of the jet, defined

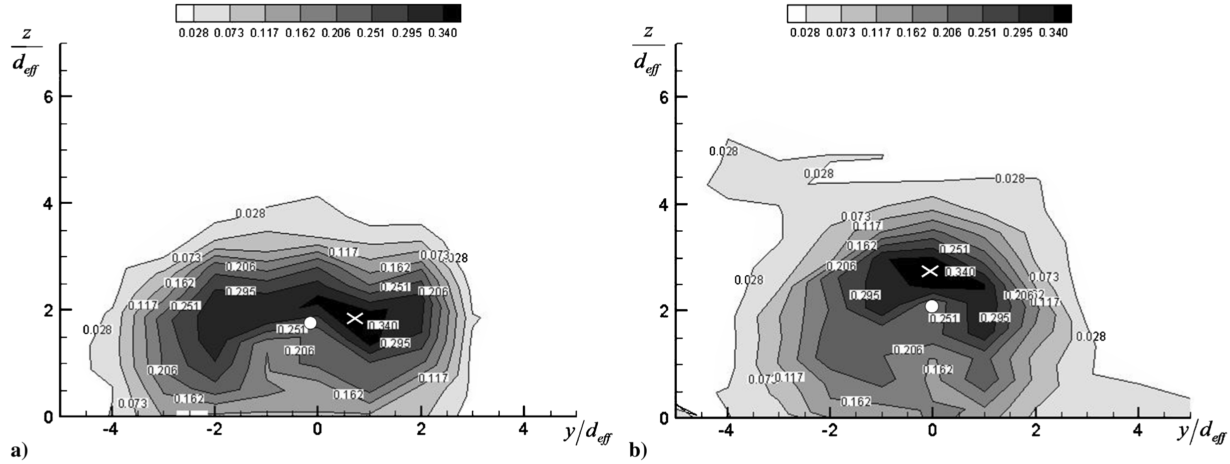

Fig. 5 Experimental results: a) aeroramp (left) and b) single-hole injectors mass-fraction contours α.

by the maximum helium mass fraction, is located at approximately $y/d_{\mathrm{eff}} = 0.68$ at an elevation of $z/d_{\mathrm{eff}} = 1.8$. Figure 5b is the jet cross section for the single-hole injector. The core of the jet is above the injector centerline at an elevation of $z/d_{\mathrm{eff}} = 2.73$. The core of the jets, for both injectors, is inside the boundary layer. At this axial location the boundary layer is about 20 mm (6 d_{eff}) as determined in the shadowgraphs.

Inspection of Fig. 5 shows a wider injectant spread for the aeroramp and a higher penetration for the single-hole injector. The profiles show the aeroramp having approximately the same maximum mass fraction and plume area as the single-hole injector, and they also qualitatively show the same mixing extent. Results for these items will be presented subsequently. For the single-hole injector, the characteristic horseshoe-shaped structure of the plume, associated with a vortex generated by the jet/freestream interaction, is beginning to appear at the measurement plane. The aeroramp, on the other hand, produces a wide horizontal region of maximum mass fraction, at approximately a constant height of $\sim 2\,d_{\mathrm{eff}}$. In general, the aeroramp injector generates vorticity not only by jet-freestream interaction, but also from the combined effects of the multiple jet interaction, the toe-in angles of the jets, and additional vorticity generated by the multiple jet bow shocks (Crocco's theorem). In the present investigation, there is no evidence of a significant counter-rotating axial vortical motion, usually identified by the formation of two primary cores.

D. Jet Interaction Characteristics

A quantifiable measure of the penetration of the fuel plume into the main flow is given by the location of the center of mass in a cross-sectional plane $(y - z)$ of the flow[25]

$$z^{+} = \frac{\int \rho u \alpha z \,\mathrm{d}A}{\int \rho u \alpha \,\mathrm{d}A} \tag{8}$$

The results presented in Table 1 show the single-hole injector penetrates higher than the aeroramp, as expected, based on the higher initial momentum value in the z direction. Table 1 also presents the results for the plume width $y^{\pm}$ defined by the distance between the plume core and the stoichiometric side edges, respectively. The aeroramp produces a significantly larger amount of lateral mixing.

The overall plume area is defined here as the total area of the plume that has an α greater or equal to the stoichiometric value for hydrogen, namely, 0.0292. Results from this study are presented in Table 1. The overstoichiometric-plume areas are normalized by A_u, the area of an isentropically expanded jet with a static pressure equal to that of the freestream. The results show that the overstoichiometric-plume area of the aeroramp injector array is larger than that of the single-hole injector.

In a nonreacting simulation of a supersonic combustor, it is useful to know the mixing efficiency of the injection process. This predicts how well the fuel would burn in an actual scramjet combustor with the same pressure field. The mixing efficiency η_m is the total mass of fuel that would react assuming steady, isentropic, quasi-one-dimensional flow divided by the total mass flow rate of fuel. This is given by[26]

$$\eta_m = \frac{\int \rho u Z \,\mathrm{d}A}{\int \rho u \alpha \,\mathrm{d}A} \tag{9}$$

where $Z = \alpha$, if $\alpha \leq f$ (H_2 lean—all H_2 consumed) or $Z = (1 - \alpha) f/(1 - f)$ if $\alpha > f$ ($\mathrm{O_2}$ lean—all $\mathrm{O_2}$ consumed).

Table 1 presents the results, which show that the mixing efficiency value of the aeroramp injector model is slightly higher than that for the single-hole injector.

The injectant mass flow [denominator of Eq. (9)] was compared with the injectant mass flow rate actually measured during the experiments. This analysis shows the uncertainty in conservation of mass of +17 to −18% for the single-hole injector and the aeroramp, respectively. One cause for this uncertainty is the relatively sparse grid spacing of the measurements. Other causes include errors in deducing ρ, u, and α as described earlier.

E. Mach Number Contours

Once the local mass fraction is known, it is possible to calculate the Mach-number. Mach-number contours of the injectors flow-fields are shown in Fig. 6. The Mach number is about equal to its freestream value at the top of the profile. Each contour has a point corresponding approximately to the edge of the jet. The sharp decrease in Mach number is caused by mixing of low-Mach-number gas from the jets with the higher-Mach-number gas from the freestream, viscous forces in the boundary layer, and the variation of the jet bow shock strength.

VI. Computational Studies

Computational fluid dynamics (CFD) is an analysis tool that has the ability to allow a more detailed and thorough study of local phenomena as well as predict the overall behavior of the flow. This work attempts to validate a Reynolds-averaged Navier–Stokes (RANS) model for foreign gas jet injection into a freestream flow of Mach 4. In addition, comparisons of the aeroramp injector and the single-hole injector to experiment and each other will be made. The general aerodynamic simulation program (GASP) flow solver was used for the analysis.

The CFD model mimics the experimental setup for both the single-hole injector and the aeroramp injector. The tunnel approach flow creates a weak shock at a joint on the tunnel surface before the injectors are reached. The shock slows the flow to Mach 3.6. As a result, Mach 3.6 was used in computing the inflow boundary conditions for the CFD models. The freestream flow is at a pressure of 11,774 Pa and a temperature of 82 K, and the helium is injected at

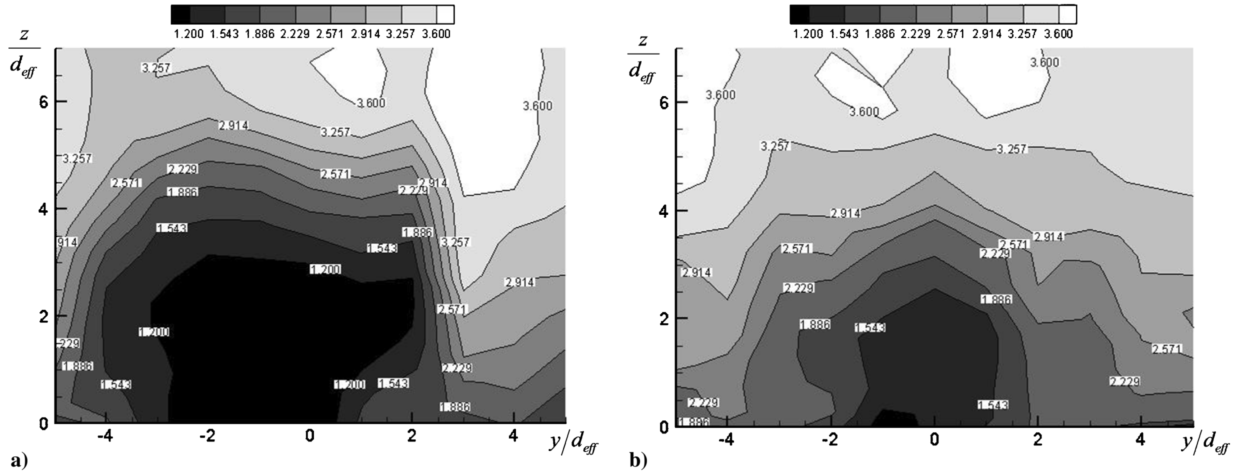

Fig. 6 Experimental results: a) aeroramp and b) single-hole injector Mach-number contours. Axis are normalized by d_{eff}.

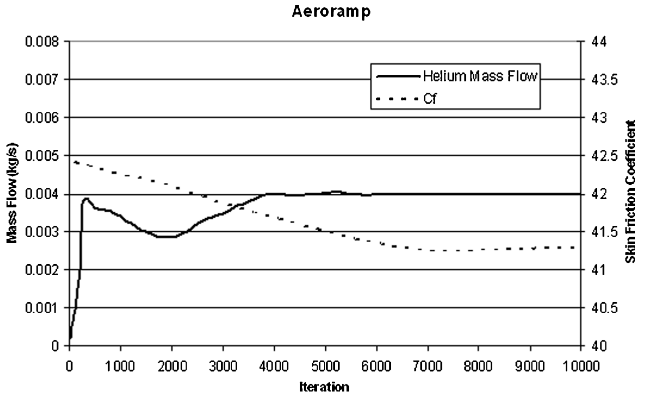

Fig. 7 Aeroramp injector convergence behavior.

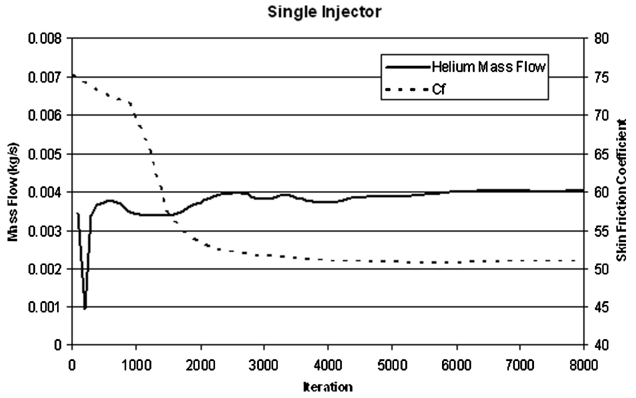

Fig. 8 Single-hole injector convergence behavior.

Mach 1.0, a temperature of 234 K, and a pressure of 224,634 Pa. The pressure and density were adjusted to match for the experimental mass flow rate. The computational domain extends five diameters down into the plenum chamber of the injectors in order to more accurately represent the flow conditions entering the freestream.

Boundary conditions were applied to the inflow (known freestream conditions); injector inflow (known He conditions); injector walls (tangency); bottom surface (no-slip, adiabatic wall); and the top, sides, and outflow (first-order extrapolation).

The calculations were run on a Linux cluster using 80 nodes with 1.4-GHz Opteron processor, 1.6-GB memory and 10-GB hard drive each. The aeroramp and single-hole injectors were run to steady state.

A. Grid Topology

All grids were created using Gridgen v.13.3 (see Ref. 27). The grid was clustered in the near-wall region in order to capture the boundary layer and steep gradients. A grid study was performed comparing a strictly H-type, grid and a combination of C-type, O-type, and H-type grids that mimicked the flow behavior. By shaping the grid to map the flow, the cells were skewed especially in the near-wall region behind the injectors, and the zonal boundaries had a larger effect on the CFD predictions so that approach was abandoned. Also, the final H-type grids were designed without a symmetry plane as a result of erroneous spikes created by the original grid in the area near the symmetry plane boundary condition.

The final grid for the aeroramp injector consisted of 5.3 million cells with an initial Δy of 2×10^{-6}, which gave a y^+ of less than 1.0 in the boundary layer. The grid was sequenced once. Each sequence was run until convergence was achieved as can be found in Fig. 7. Mass flow of helium and the X and Y forces on the bottom surface were used a convergence parameters. The cases were run until there was consistentl less than a 0.5% difference in the parameters.

Boundary conditions were applied to the inflow (freestream conditions), injector inflow (known conditions of the He), the injector plenum walls (tangency), the bottom surface of the domain (no-slip, adiabatic) and the sides, top and outflow of domain (first-order extrapolation).

The single-hole injector grid had 5.6 million cells and was sequenced once. The final H-type grid for the single-hole injector had an initial Δy of 3×10^{-6}, which gave a y^+ of less than 1.0 in the boundary layer. Figure 8 shows the convergence behavior for the single-hole injector grid. The cases were run until there was consistently less than a 0.5% difference in the parameters.

B. GASP Flow Solver

The GASP[28] Version 4.2 flow solver is a time-dependent, three-dimensional, RANS solver. It solves the integral form of the governing equations using upwind-based, finite volume formulations. GASP supports multiblock, structured grid topologies. Steady-state solutions are marched in time using local time stepping, whereas time-accurate flows are solved using a dual-time stepping procedure. In this study, the implicit Gauss–Seidel scheme was used. The inviscid fluxes were computed in three dimensions using third-order Roe FDS with min-mod limiting. The Roe algorithm was chosen because the algorithm produces good resolution of shock discontinuities and it shows efficiency. The Wilcox k-ω (1998) turbulence model was used. Of the viable options for two-equation turbulence models within GASP, the Wilcox k-ω (1998) model has been successfully used to model supersonic flows.

VII. Computational Results

A. Helium Concentration

The helium concentration contours found in Figs. 9 and 10 show that the CFD predicts slower mixing of helium than the experiment

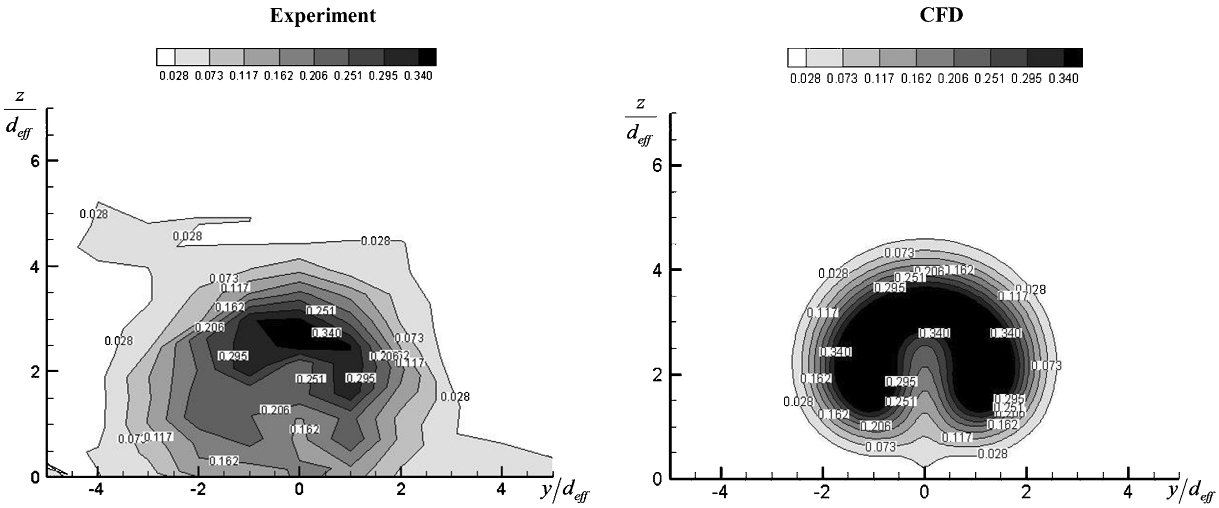

Fig. 9 Measured and predicted helium concentration contours in the $x/d_{\mathrm{eff}} = 16.4$ plane for the single-hole injector.

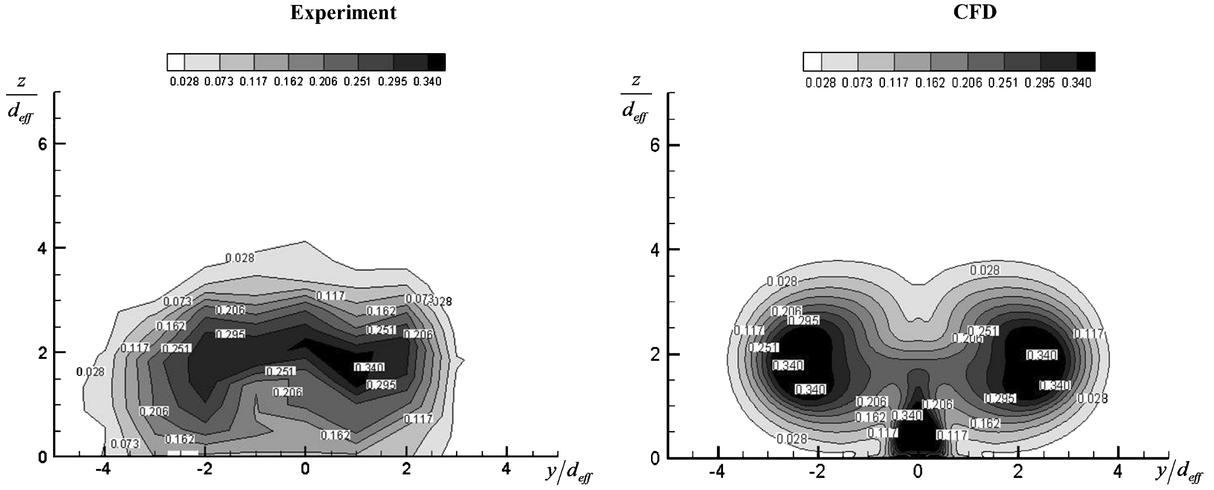

Fig. 10 Measured and predicted helium concentration contours in the $x/d_{\mathrm{eff}} =$ plane of the aeroramp injector.

because there is a larger area of maximum concentration. The contours are slices in the y-z plane taken at x/d_{eff} of 16.4. The maximum predicted concentration for the single-hole injector was 0.65 located at $y/d_{\mathrm{eff}} = 1.16$ and $z/d_{\mathrm{eff}} = 2.24$ (experiment: 0.358 at $y/d_{\mathrm{eff}} = 0$ and $z/d_{\mathrm{eff}} = 2.73$). The maximum concentration for the aeroramp injector was 0.43 located at $y/d_{\mathrm{eff}} = 1.95$ and $z/d_{\mathrm{eff}} = 2.49$ (experiment: 0.352 at $y/d_{\mathrm{eff}} = 0.68$ and $z/d_{\mathrm{eff}} = 1.7$). The single-hole injector mixes more slowly than the aeroramp injector. The maximum concentration predicted by CFD for the aeroramp injector agrees more closely with the experiment than the maximum concentration predicted for the single-hole injector. The single-hole injector penetrates further in the vertical direction, but the aeroramp penetrates significantly further in the transverse direction. The experiment and CFD predict a horseshoe shape of concentration for the single-hole injector with similar vertical penetration. The CFD predicts less lateral penetration than the experiment. Also, CFD predicts the concentration plume to be lifted completely off the surface.

The aeroramp injector prediction has two distinct plume cores, which show evidence of two counter-rotating vorticies. The experiment shows a more connected plume on the centerline than the CFD predictions. The vertical penetration and lateral penetration are similar between the two contours. The CFD predictions show less concentration of helium on the surface in the boundary layer. CFD predicts a higher maximum concentration, but the gradient of concentration is similar to the experimental results.

B. Total Temperature Contours

The total temperature contours can be found in Figs. 11 and 12. The single-hole injector contours for both the experiment and CFD show the same horseshoe shape, although the CFD predicts a higher total temperature and steeper gradient between high and low total temperatures. The CFD for both the single-hole injector and the aeroramp injector predict an area of higher total temperature fluid surrounding a small area of lower total temperature fluid. The experiment does not show the same result, and the overall area with a varying total temperature is smaller in the CFD predictions. The single-hole injector penetrates further in the vertical direction, whereas the plume from the aeroramp injector spreads further laterally.

The CFD and experiment results for the aeroramp injector show an area of lower total temperature in the center of two higher total temperature cores than the single injector. CFD predicts slower mixing than the experiment. This is shown by the two large areas of high total temperature off center. There is an area of lower temperature fluid on the centerline of both the CFD and experiment for the aeroramp injector.

C. Mach Number

Predicted contours of the Mach number compared to experiment can be found in Figs. 13 and 14. CFD predicts a smaller area of slower moving fluid and a higher overall Mach numbers than the experiment. The dips near the side of the contour plots evident in the experimental results are not predicted by CFD. The single-hole

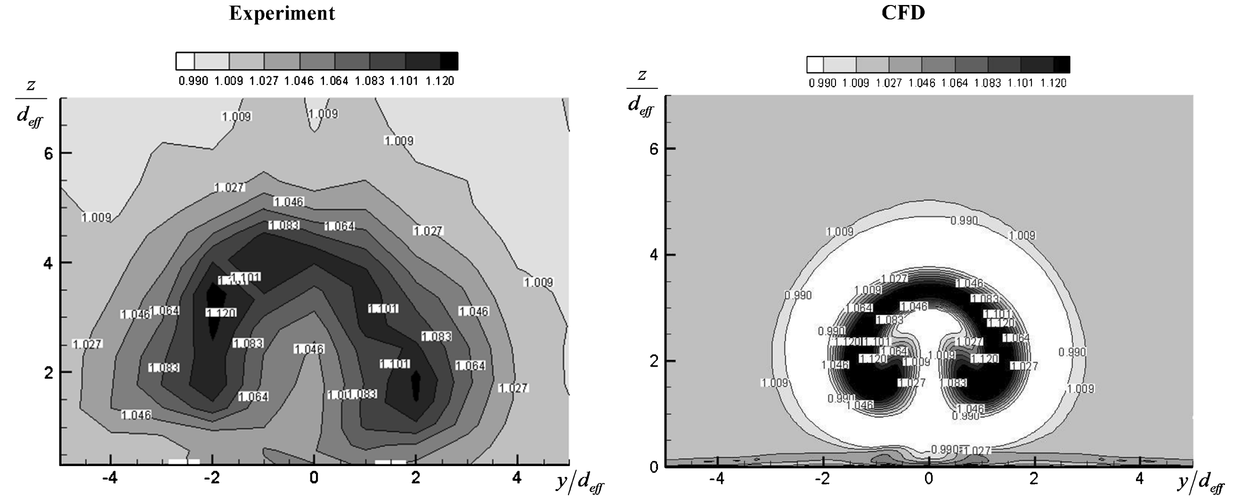
Experiment

CFD

Fig. 11 Predicted and measured normalized total temperature ratio in the $x/d_{\text{eff}} = 16.4$ plane for the single-hole injector.

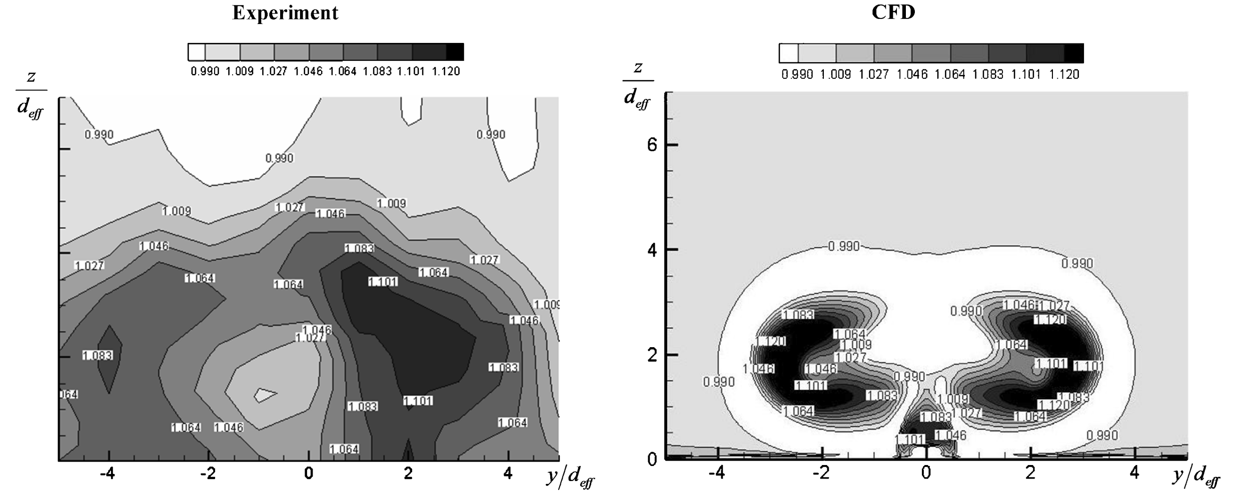
Experiment

CFD

Fig. 12 Predicted and measured normalized total temperature ratio in the $x/d_{\text{eff}} = 16.4$ plane for the aeroramp injector.

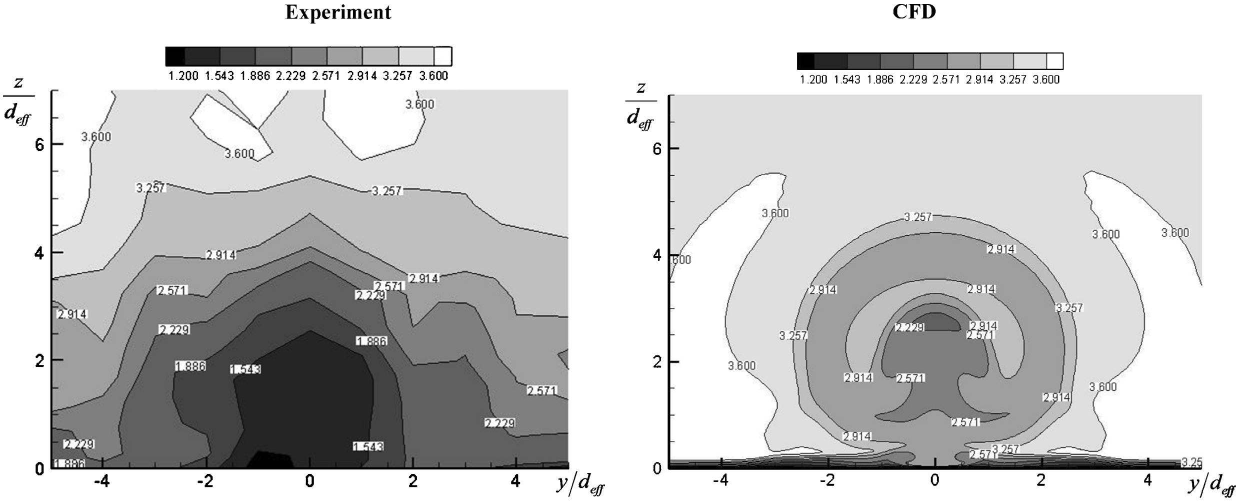
Experiment

CFD

Fig. 13 Calculated and measured Mach-number contours in the $x/d_{\text{eff}} = 16.4$ plane of the single-hole injector.

injector penetrates higher in the vertical direction, and the aeroramp injector has a larger area of lower-speed fluid in the lateral direction. The feature on the centerline, at approx $z/d_{\text{eff}} = 4.5$, of the contour in the CFD prediction of the aeroramp injector is not a result of the grid. It could be a consequence of the two three-dimensional counter-rotating vorticies created by the aeroramp injectors. The vorticies trap slower moving fluid on the centerline and carry it in the vertical direction. Some of the fluid continues to rotate with the vorticies, while some of the fluid is pushed further in the vertical direction.

D. Total Pressure Ratio

The predicted total pressure was normalized by the freestream total pressure and then used with the normal-shock relations to create plots of the pitot pressure, P_{T2} (i.e., the total pressure measured using a hypothetical pitot probe in the computed flow). The resultant

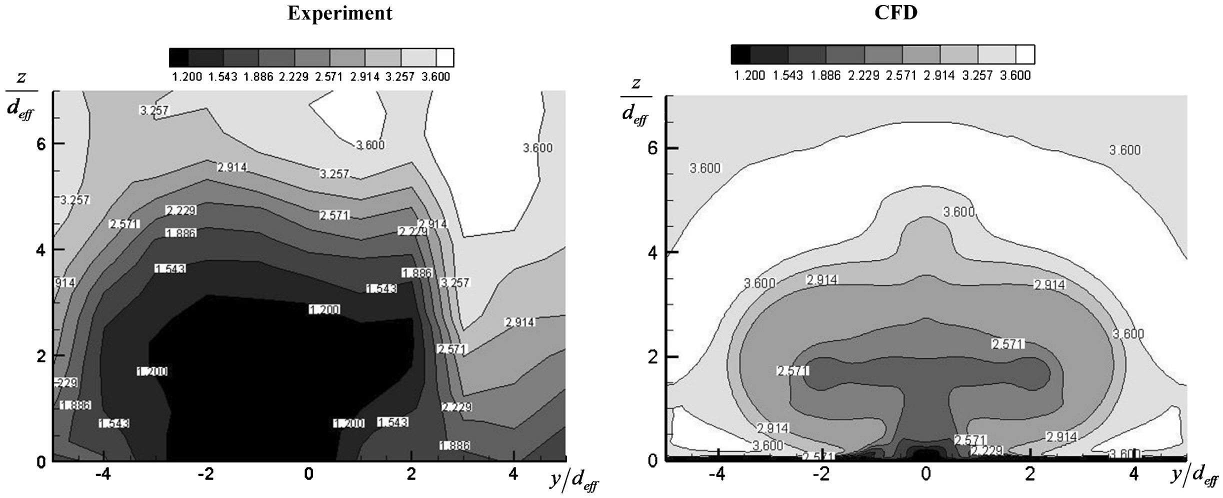

Fig. 14 Calculated and measured Mach-number contours in the $x/d_{\mathrm{eff}} = 16.4$ plane of the aeroramp.

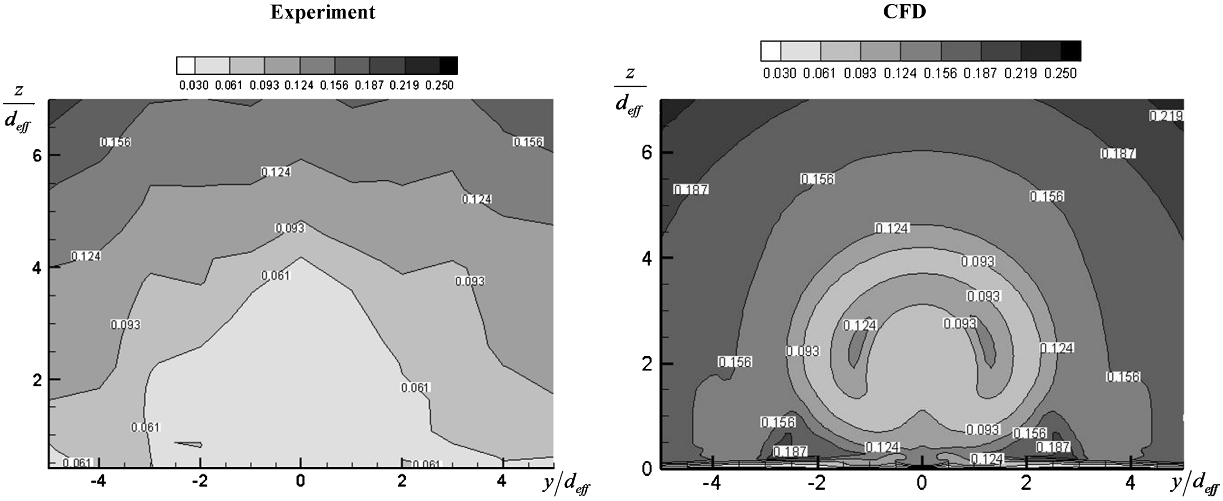

Fig. 15 Normalized pitot total pressure ratio in the $x/d_{\mathrm{eff}} = 16.4$ plane of the single injector.

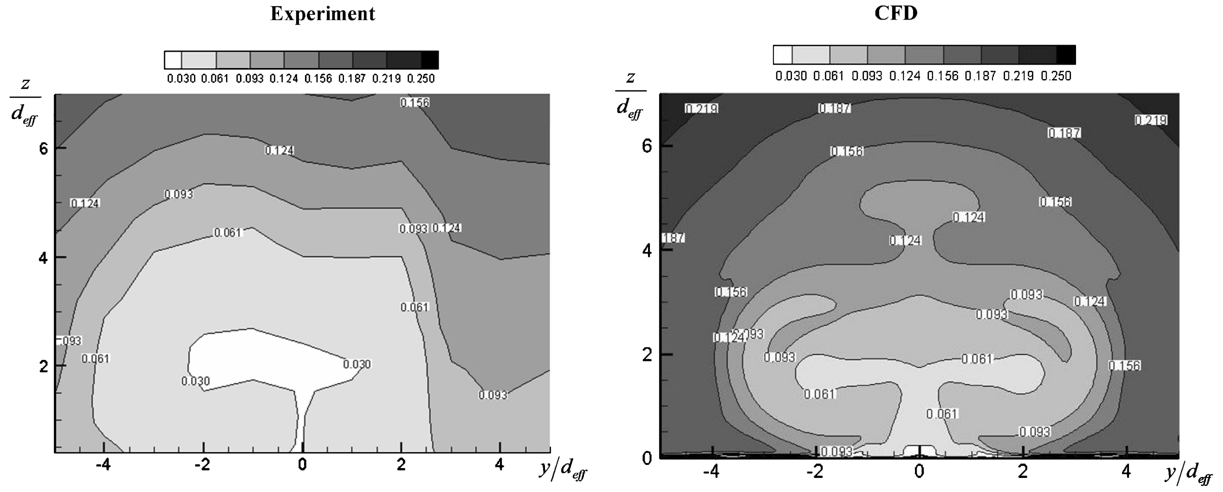

Fig. 16 Predicted and measured normalized pitot total pressure ratio in the $x/d_{\mathrm{eff}} = 16.4$ plane of the aeroramp injector.

contours can be found in Figs. 15 and 16. The pitot pressure was used as a comparison with CFD because there are fewer data-reduction steps involved in the measurement and therefore less room for error when comparing the contours. The CFD predictions for the aeroramp injector agree more closely with the experiment than the predictions for the single-hole injector. There is a larger area of low-pressure gas in the aeroramp injector contour than in the single-hole injector contour. The low-pressure gas extends further laterally for the aeroramp injector than for the single-hole injector, but the single-hole injector has more low-speed fluid in the vertical direction. CFD predicts the plumes to be pulled off the surface, whereas the experimental results show a large area of low-pressure gas in the boundary layer. The feature on the centerline of the aeroramp injector contour that was evident in the Mach contours is seen in the total pressure contours. The low-pressure gas is being rotated up away from the surface and partially dispersed into the freestream. The aeroramp

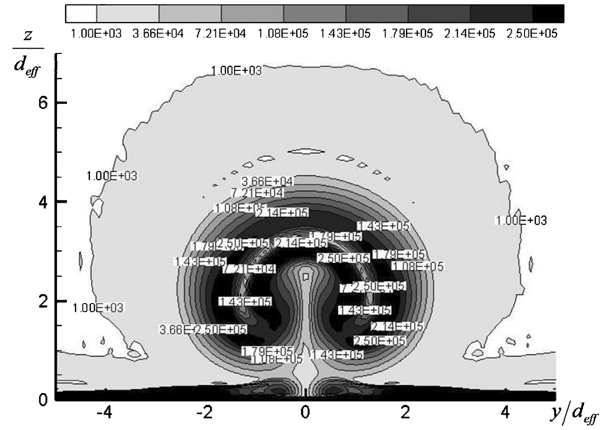

Fig. 17 Predicted vorticity ratio in the $x/d_{\mathrm{eff}} = 16.4$ plane for the single-hole injector.

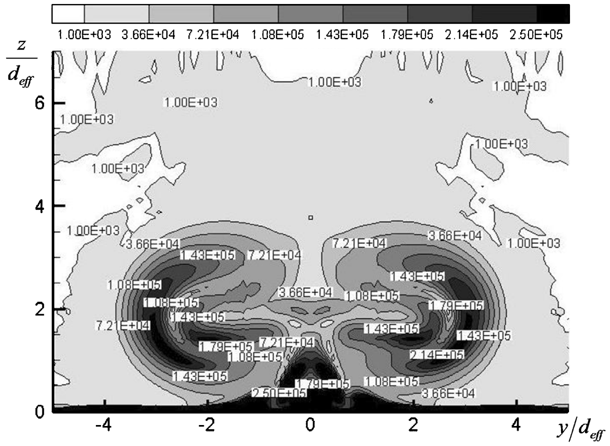

Fig. 18 Predicted vorticity ratio in the $x/d_{\mathrm{eff}} = 16.4$ plane for the aeroramp injector.

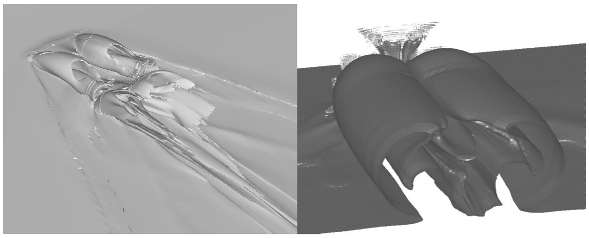

a) $\omega = 800{,}000/\mathrm{s}$ **b) $\omega = 50{,}000/\mathrm{s}$**

Fig. 19 Isosurfaces for the aeroramp injector at two vorticity levels.

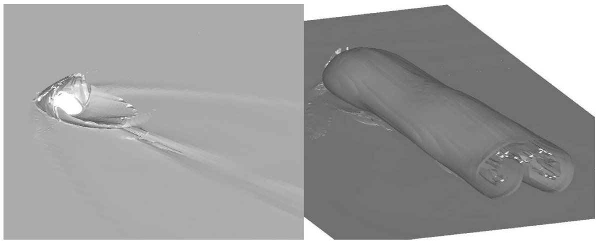

a) $\omega = 800{,}000/\mathrm{s}$ **b) $\omega = 100{,}000/\mathrm{s}$**

Fig. 20 Isosurfaces for the single-hole injector at two vorticity strengths.

contour CFD prediction shows the low-pressure gas beginning to rotate away from the centerline and back towards the surface. The rotation of the low-pressure gas found in the CFD predictions is not shown in the experimental results.

Using Eq. (7), the total pressure loss parameter was calculated. The predicted total pressure was used, not the pitot pressure, for this calculation. The result for the aeroramp injector was 0.41 and for the single injector was 0.398. These values are similar to the experimental results. The aeroramp predicts a higher total pressure loss than the single injector, which follows the same trend as predicted by the experiment.

E. Vorticity

Vorticity was not measured in the experiment, but CFD can produce useful results for that important flow variable. Predicted vorticity magnitude contours in the $x/d_{\mathrm{eff}} = 16.4$ plane can be found for the single-hole injector in Fig. 17 and for the aeroramp injector in Fig. 18. Vortex flow enhances mixing through entrainment of freestream fluid and enhanced strain rates on the shear layer, which increase the local diffusion gradients. The aeroramp injector mixes faster than the single injector by creating a larger interfacial surface area to entrain the freestream fluid. The aeroramp not only has freestream air on the outside of the injector system, but it traps freestream air in between the four injectors. The air is then mixed with the injected helium. The single-hole injector creates a horseshoe contour that is to be expected of a jet in a crossflow. The single-hole injector appears to pull the helium away from the surface better than the aeroramp injector; however, the aeroramp has less vorticity in the boundary layer and in the plumes as a result of improved mixing. The aeroramp injector has two contour-rotating vortices that rotate away from the surface and away from the centerline. The two vorticies mix the helium at a faster rate and diffuse the vorticity into the flow.

Figure 19 shows vorticity isosurfaces for various levels of vorticity. Behind the first set of injectors in the aeroramp configuration, the existing vorticity encounters the vorticity created by the second set of injectors and appears to bend around or above it. Figure 19b depict the shape of two levels of vorticity. The vorticity appears to create two smooth outer surfaces surrounding the inner rotating cores.

The single-hole injector isosurfaces (Fig. 20) depict the rotating behavior of the plume. The injected gas is lifted up the centerline off the surface and then rotates in both directions away from the centerline. The gas is mixed with the freestream as it rotates. The single-hole injector has a higher vorticity magnitude and a smaller plume of vorticity than the aeroramp injector.

VIII. Discussion

Experiments were performed at Virginia Polytechnic Institute and State University to investigate the behavior of a four-hole aeroramp injector previously developed and studied by Jacobsen et al.[23] for hydrocarbon gas injection into a Mach 2.4 airstream. The aeroramp was compared to a single, low-angled circular injector. Both injectors were exposed to a Mach 4 cross stream with heated helium as the injectant to simulate hydrogen.

Helium concentration, pitot pressure, total temperature, and cone-static measurements were taken during the mixing studies. Helium mass fraction contours, Mach number, total temperature, and total pressure plots were generated. From these data, penetration of the helium injectant core, total pressure losses, and mixing efficiency were calculated. The main conclusion drawn from these studies are as follows:

1) The mixing efficiency value of the aeroramp was only slightly higher than that of the single-hole injector at these conditions.

2) The aeroramp injector showed somewhat higher local total pressure losses at some places in the plume than the single-hole injector. This was because of the higher angle of injection of the first row of the aeroramp array and the multiple shock structures from the two rows of jets. Although the local total pressure losses appeared more substantial, the mass averaged total pressure

loss parameter showed that the aeroramp had the same overall losses.

3) The aeroramp had a plume area comparable with the plume area of the single-hole injector. The aeroramp produced a larger amount of lateral mixing. This was because of the greater cross-stream distance between the individual injector holes and more rapid mixing.

4) The core of the jet, that is, location at maximum helium mass fraction, was higher for the single-hole injector as expected considering the higher initial momentum value in the z direction.

5) The present aeroramp was optimized for the injection of ethylene in a Mach 2.4 crossflow. Further development might include a study of the optimization of the aeroramp injector design for higher-Mach-number conditions with light gas injections.

6) The CFD based on a RANS formulation with a k-ω turbulence model was able to predict the behavior and trends in the flow. Although the CFD predictions were similar, the experimental results for the mass fraction contours, the total pressure, total temperature, and Mach-number contours were not as accurately predicted. The choice of turbulence model could play a large role in the discrepancies between the experiment and the CFD predictions. The aeroramp injector predicted faster mixing and a larger lateral penetration than the single-hole injector. The aeroramp injector also predicted a larger low-pressure, low-speed region around the centerline.

7) Possible improvements in the CFD predictions could be found by adding freestream turbulence to the model. Turbulence upstream of the injector(s) in the experiment will increase mixing.

The effects of compressibility in the formation and development of turbulent structures in simple shear layers can be categorized using a nondimensional parameter, the convective Mach number M_c. This is a key compressibility parameter, which is based on the velocity of the large structures relative to a freestream. Papamopschou and Rosko[29] defined a convective Mach number for each stream:

$$M_{c1} = (U_1 - U_c)/a_1, \qquad M_{c2} = (U_c - U_2)/a_2 \tag{10}$$

where U_1 and U_2 are the high- and low-speed velocities. An isentropic pressure balance, with $p_1 = p_2$ (static pressure) and $\gamma_1 = \gamma_2$, yields $M_{c1} = M_{c2}$ and

$$M_{c1} = M_{c2} = (U_1 - U_2)/(a_1 + a_2) \tag{11}$$

Furthermore, it can be shown that M_{c1} and M_{c2} are still fairly close even when $\gamma_1 \neq \gamma_2$, provided that $p_1 \simeq p_2$. As shown by Papamopschou and Rosko, growth rates of mixing layers are suppressed with increasing convective Mach number, which is associated with a turbulent structure becoming fully three dimensional. One could adapt the convective Mach-number concept to scale the compressibility of transverse jets. One way is as suggested by Ben-Yakar et al.[30] For the conditions of the present investigation, M_c is greater than the M_c calculated for the earlier aeroramp case of $M = 2.4$ with heated air injection,[31] which performed well. This might help to explain the decreased performance obtained here.

If we assume a constant characteristic time, defined as

$$t^* = \ell/U_c \tag{12}$$

where ℓ is a characteristic length (i.e., the distance between the orifices) and U_c is the convective velocity, it is possible to scale the geometry of the aeroramp injector for a new set of operation conditions because:

$$U_c = U_c(M_\infty, \bar{q}) \tag{13}$$

Following this procedure, we predict for $M = 4$ and helium injection the need to increase the distance in the spanwise direction between the orifices of the aeroramp with respect to the initial configuration. Studies to support this approach are planned.

Acknowledgments

This research was supported by the Air Force Office of Scientific Research under a MURI lead by Paul Dimotakis at Caltech and by the Defense Advanced Research Projects Agency, under a project lead by Michael Holden at CUBRC. Frederick Billig provided helpful guidance throughout.

References

[1] Hartfield, R. J., Hollo, S. D., and McDaniel, J. C., "Experimental Investigations of a Supersonic Swept Ramp Injector Using Laser Induced Iodine Fluorescence," *Journal of Propulsion and Power*, Vol. 10, No. 1, 1994, pp. 129–135.

[2] Riggins, D. W., and Vitt, P. H., "Vortex Generation and Mixing in Three-Dimensional Supersonic Combustors," *Journal of Propulsion and Power*, Vol. 11, No. 3, 1995, pp. 419–426.

[3] Lewis, D. P., and Schetz, J. A., "Tangential Injection from Overlaid Slots into a Supersonic Stream," *Journal of Propulsion and Power*, Vol. 13, No. 1, 1997, pp. 59–63.

[4] Schetz, J. A., Billig, F. S., Favin, S., and Gilreath, H. E., "Effects of Pressure Mismatch on Slot Injection in a Supersonic Flow," *International Journal of Turbo and Jet Engines*, Vol. 9, No. 2, 1992, pp. 135–146.

[5] Tomioka, S., Jacobsen, L. S., and Schetz, J. A., "Interaction Between a Supersonic Airstream and a Sonic Jet Injected Throught a Diamond-Shaped Orifice," AIAA Paper 2000-0088, Jan. 2000.

[6] Schetz, J. A., "Interaction Shock Shape for Transverse Injection," *Journal of Spacecraft and Rockets*, Vol. 7, No. 2, 1970, pp. 143–149.

[7] Fuller, E. J., Mays, R. B., Thomas, R. H., and Schetz, J. A., "Mixing Studies of Helium in Air at Mach 6," AIAA Paper 91-2268, June 1991.

[8] Barber, M. J., Roe, L. A., and Schetz, J. A., "Simulated Fuel Injection Through a Wedge Shaped Orifice in a Supersonic Flow," AIAA Paper 95-2559, July 1995.

[9] McClinton, C. R., "The Effect of Injection Angle on the Interaction Between Sonic Secondary Jets and a Supersonic Freestream," NASA TND-6669, Feb. 1972.

[10] Rogers, R. C., "A Study of the Mixing of Hydrogen Injected Nomal to a Supersonic Airstream," NASA TN L-7386, March 1971.

[11] Jacobsen, L. J., Schetz, J. A., Gallimore, S. D., and O'Brian, W. F., "Mixing Enhancement by Jet Swirl in a Multiport Injector Array in Supersonic Flow," FEDSM99-7448, July 1999.

[12] Kraus, D. K., and Cutler, A. D., "Mixing of Swirling Jets in a Supersonic Duct Flow," *Journal of Propulsion and Power*, Vol. 12, No. 1, 1996, pp. 170–177.

[13] Cutler, A. D., and Johnson, C. H., "The Use of Swirling Jet Pairs to Provide Rapid Fuel Penetration in Scramjet Combustors," AIAA Paper 95-0099, Jan. 1995.

[14] Schetz, J. A., *Injection and Mixing in a Turbulen Flow*, AIAA, New York, 1980.

[15] Povinelli, L. A., and Ehlers, R. C., "Swirling Base Injection for Supersonic Combustion Ramjets," *AIAA Journal*, Vol. 10, No. 9, 1972, pp. 1243, 1244.

[16] Schetz, J. A., and Swanson, R. C., "Turbulent Jet Mixing at High Supersonic Speeds," Zeitschrift fur flugwissen schaften, Vol. 21, 1973, pp. 166–173.

[17] Schetz, J. A., Thomas, R. H., and Billig, F. S., "Separated Flows and Jets," edited by V. V. Koshow and A. V. Dougal, Springer-Verlag, Berlin, 1991, pp. 807–837.

[18] Cox, S. K., Fuller, R. P., and Schetz, J. A., "Vortical Interactions Generated by a Injector Array to Enhance Mixing in a Supersonic Flow," AIAA Paper 94-0708, Jan. 1994.

[19] Cox, S. K., and Gruber, M. R., "Effects of Spanwise Injector Spacing on Mixing Characteristic of Aerodynamic Ramp Injectors," AIAA Paper 98-3272, July 1998.

[20] Fuller, R. P., Nejad, A. S., and Schetz, J. A., "Fuel-Vortex Interactions for Enhancing Mixing in Supersonic Flow," AIAA Paper 96-2661, July 1996.

[21] Schetz, J. A., Cox-Stouffer, S., and Fuller, R., "Integrated CFD and Experimental Studies of Complex Injectors in Supersonic Flows," AIAA Paper 98-2780, June 1998.

[22] Jacobsen, L. S., Gallimore, S. D., Schetz, J. A., and O'Brien, W. F., "Integration of an Aeroramp Injector/Plasma Igniter for Hydrocarbon Scramjets," *Journal of Propulsion and Power*, Vol. 19, No. 2, 2003, pp. 170–182.

[23] Jacobsen, L. S., Gallimore, S. D., Schetz, J. A., O'Brien, W. F., and Goss, L. P., "Improved Aerodynamic-Ramp Injector in Supersonic Flow," AIAA Paper 2001-0518, Jan. 2001.

[24] Ng, W. F., Kwok, F. T., and Ninnemann, T. A., "A Concentration Probe for the Study of Mixing in Supersonic Shear Flows," *Experiments in Fluids*, Vol. 13, 1992, pp. 98–104.

[25] Doerner, S. E., and Cutler, A. D., " Effects of Jet Swirl on Mixing of a Light Gas Jet in a Supersonic Airstream," NASA/CR-1999-209842, Dec. 1999.

[26] Mao, M., Riggins, D. W., and Mc Clinton, C. R., "Numerical Simulation of Transverse Fuel Injection," NASP CR 1089, May 1990.

[27] Gridgen ver. 13.3 User Manual, Pointwise, Inc., Bedford, TX, 2004.

[28] GASP Version 4 Technical Reference, AeroSoft, Inc., Blacksburg, VA.

[29] Papamopschou, D., and Roshko, A., "The Compressible Turbulent Shear Layer: an Experimental Study," *Journal of Fluid Mechanics*, Vol. 197, 1988, pp. 453–477.

[30] Ben-Yakar, A., Mungal, M. G., and Hanson, R. K., "Transverse Jets in Supersonic Crossflow, Part 2: The Effect of Compressibility, Velocity Ratio and Density Ratio," *Physics of Fluids* (submitted for publication).

[31] Jacobsen, L. S., Gallimore, S. D., Schetz, J. A., O'Brien, W. F., and Goss, L. P., "Improved Aerodynamic-Ramp Injector in Supersonic Flow," *Journal of Propulsion and Power*, Vol. 19, No. 4, 2003, pp. 663–673.